ORIGINAL PAPER

Lithiation/delithiation performance of Sn–Co alloy anode using rough Cu foil as current collector

Xiao-Yong Fan · Fu-Sheng Ke · Guo-Zhen Wei · Ling Huang · Shi-Gang Sun

Abstract Sn–Co alloys were electrodeposited on the rough Cu foil and smooth Cu sheet, respectively. The capacity retention of the Sn–Co alloy electrode electrodeposited on the rough Cu foil in the 70th cycle was found to be 80.0% compared with the maximal capacity, which was much better than that of the Sn–Co alloy electrode on the smooth Cu sheet. The revolution of the surface morphology of the Sn–Co alloy electrode during cycling was investigated by scanning electron microscopy. The result indicated that the reversibility of the expansion and contraction of the Sn–Co alloy electrode on the rough Cu foil during charging/discharging assisted by the unique rough surface was one main reason of improving the cycleability. Solid electrolyte interphase (SEI) film was detected on the Sn–Co alloy electrode surface by electrochemical impedance spectroscopy (EIS) during lithiation/delithiation, and the result demonstrated that the SEI film suffered breaking and repairing at different lithiation status. In addition, the unique phase transformation process for the Sn–Co alloy electrode during first lithiation was also investigated by EIS.

Keywords Lithium-ion battery · Sn–Co alloy · Rough Cu foil · Phase transformation impedance

X.-Y. Fan
School of Materials Science and Engineering,
Chang'an University, Xi'an 710061, China

X.-Y. Fan · F.-S. Ke · G.-Z. Wei · L. Huang · S.-G. Sun (✉)
State Key Lab of Physical Chemistry of Solid Surfaces,
Department of Chemistry,
College of Chemistry and Chemical Engineering,
Xiamen University, Xiamen 361005, China
e-mail: sgsun@xmu.edu.cn

Introduction

In lithium-ion battery technology, there is continuing demand for new electrode materials with higher energy density and specific capacity compared with conventional anode and cathode materials of graphite and $LiCoO_2$, respectively. For replacing the graphite anode used in the commercial lithium-ion battery, many Li alloy electrodes especially Li–Sn alloy electrodes have been extensively researched [1, 2]. However, they have not come to practice because of large volume expansion and contraction during charging/discharging, which causes pulverization and exfoliation of active materials and consequently causes poor electrochemical cycleability [3]. Recently, a large number of investigations have indicated that when one or two active/inactive element was alloyed with Sn, such as Cu_6Sn_5 [4–8], Co_3Sn_2, CoSn, $CoSn_2$, the electrochemical cycleability can be much improved. Among these alloys, Sn–Co alloys were proved to be one of the most promising anodes for lithium-ion battery. Tamura et al. [9, 10] have electro-co-deposited Sn–Co alloy electrode (which is amorphous) on rough copper foil and found that the micro-island structure on the electrode surface could improve the capacity and cycleability. Zhang and Xia [11] have prepared different intermetallic compounds such as Co_3Sn_2, CoSn, and $CoSn_2$ and found that the electrochemical reaction of lithium with crystalline $CoSn_2$ alloy resulted in the formation of Li-rich tin phase ($Li_{4.4}Sn$) with high capacity, whereas the crystalline Co_3Sn_2 and CoSn alloys only partly formed Li_xSn according to the ex situ X-ray diffraction analysis and charge/discharge test results. Ionica-Bousquet et al. [12] have also studied the lithiation mechanism of $CoSn_2$ by in situ Mössbauer spectroscopy and suggested a two-step reaction mechanism. Firstly, lithium ion is inserted into the alloy and forms a solid

solution, then lithium-rich Li_xSn compounds ($x \approx 3.5$) and Co nanoparticles are formed by substitution/extraction. Although these improvements have been achieved, further study demands to understand the volume expansion and contraction mechanism of the alloy electrodes on different current collectors during electrochemical cycling in order to improve their electrochemical performance. Besides, there were few reports about the compatibility of the alloy electrodes and commercial electrolyte, especially the revolution of solid electrolyte interphase (SEI) film on the alloy electrodes surface and phase transformation process during lithiation using electrochemical impedance spectroscopy (EIS) method, which is also important for improving their electrochemical performance.

In this work, we have electrodeposited Sn–Co alloys on the rough Cu foil and smooth Cu sheet. The phenomenon of volume expansion and contraction of the Sn–Co alloy electrode on the rough Cu foil during discharging/charging as well as the mechanism of improving performance have been directly investigated by scanning electron microscopy (SEM). The SEI film, charge transfer, and phase transformation performance of the Sn–Co alloy electrode on the rough Cu foil were also studied by EIS.

Experimental

The Sn–Co alloys were electrodeposited on the rough Cu foil and smooth Cu sheet, respectively, in the solution containing 75 g L^{-1} Na$_2$SnO$_3$·3H$_2$O, 4.0 g L^{-1} CoCl$_2$·6H$_2$O, 150 g L^{-1} C$_4$H$_4$O$_6$KNa·4H$_2$O, and 25 g L^{-1} K$_3$C$_6$H$_5$O$_7$·H$_2$O. Every sample was electrodeposited for 5 min under the current density of 10 mA cm^{-2}. Before electrodepositing, the rough Cu foil and smooth Cu sheet were pretreated in acetone and acid solution to remove oil and oxide on the surface. After electrodepositing and before assembling them into batteries, the Sn–Co alloy electrodes were dried in vacuum for 24 h at 80 °C.

The morphology and surface structure of all electrodeposits were analyzed by scanning electron microscopy (LEO 1530 field emission scanning electron microscope, Oxford Instrument). The arithmetic mean roughness, R_a, of the rough Cu foil and the smooth Cu sheet measured by laser microscopy (OLS1200, Olympus Optical) were 0.0 and 0.8 μm, respectively. The crystal structure of all electrodeposits was examined by X-ray diffraction (XRD) measurements at room temperature using a X'pert PRO diffractometer using Cu Kα radiation (λ=1.5418 A) with the collection range between 20° and 90°.

Coin-type cells were assembled in an argon-filled dry glove box using Sn–Co alloy as the positive electrode and Li metal as the negative electrode and membrane celgard 2400 as the separator. The electrolyte was 1 M LiPF$_6$ in a mixture of ethylene carbonate, dimethyl carbonate, and diethylene carbonate (1:1:1 by volume, provided by Guotaihuarong, Zhangjiagang, China). The coin-type cells were galvanostatically charged and discharged in a battery test system (NEWARE BTS-610, Neware Technology, China) with a constant current density of 50 mA g^{-1}. Electrochemical impedance was carried out over a frequency range of 100 KHz to 10 mHz with a potential signal amplitude of 5 mV using a glass three-electrode cell system (Sn–Co alloy as the work electrode, Li metal as the reference and counter electrode) on PARSTAT 2263-1 (PRINCETON).

Results and discussion

Figure 1 gives the SEM images of the smooth Cu sheet (a), Sn–Co alloy (b) on the smooth Cu sheet, the rough Cu foil (c), and Sn–Co alloy (d) on the rough Cu foil. It can be observed that the surface of the Cu sheet (Fig. 1a) is very smooth, while the rough Cu foil (Fig. 1c) is characterized by many small "islands" and gaps on the surface. When the Sn–Co alloy was electrodeposited on the smooth Cu sheet (Fig. 1b) and the rough Cu foil (Fig. 1d), the surface of the electrodeposits has the similar morphology to that of the smooth Cu sheet and the rough Cu foil, respectively.

Figure 2 show XRD patterns (a) and EDS result (b) of the as-deposited Sn–Co alloy on the rough Cu foil. It can be concluded that the as-deposited alloy is mainly consisted of the intermetallic compound of CoSn$_3$ with orthorhombic structure (JCPDS card no. 00-048-1813) that is evidenced by the peaks at 29.3°, 30.5°, and 42.7°. Besides, there also appears some impure diffraction peaks at 43.6°, 49.9°, 73.1°, and 89.2°, which can be attributed to the crystal Cu (Cu foil substrate for our system) with cubic structure (JCPDS card no. 00-002-1225). The EDS result (Fig. 2b) indicates that the gravimetric and atom proportion of Sn and Co are 5.0 and 2.5, respectively, which is approximately consistent with the analysis of XRD illustrated in Fig. 2a from which the intermetallic compound of CoSn$_3$ was detected.

Figure 3 shows charge/discharge curves (a) and cycleability curves (b) of the Sn–Co alloy electrode on the rough Cu foil. It can be observed that there is a main potential plateau at ~0.22 V in the first discharging curve (Fig. 3a) and transfers to ~0.43 V starting from the second cycle and almost remains in similar shape in the following cycles. On first charge, two electrode potential plateaus at ~0.45 and ~0.6 V are observed and almost remain in the same position starting from the second cycle. The first discharge and charge capacities of the Sn–Co alloy electrode on the rough Cu foil illustrated in Fig. 3b are measured at 454.4 and 334.5 mAh g^{-1}, respectively. It can be also observed that the charge capacity of the Sn–Co alloy electrode on the
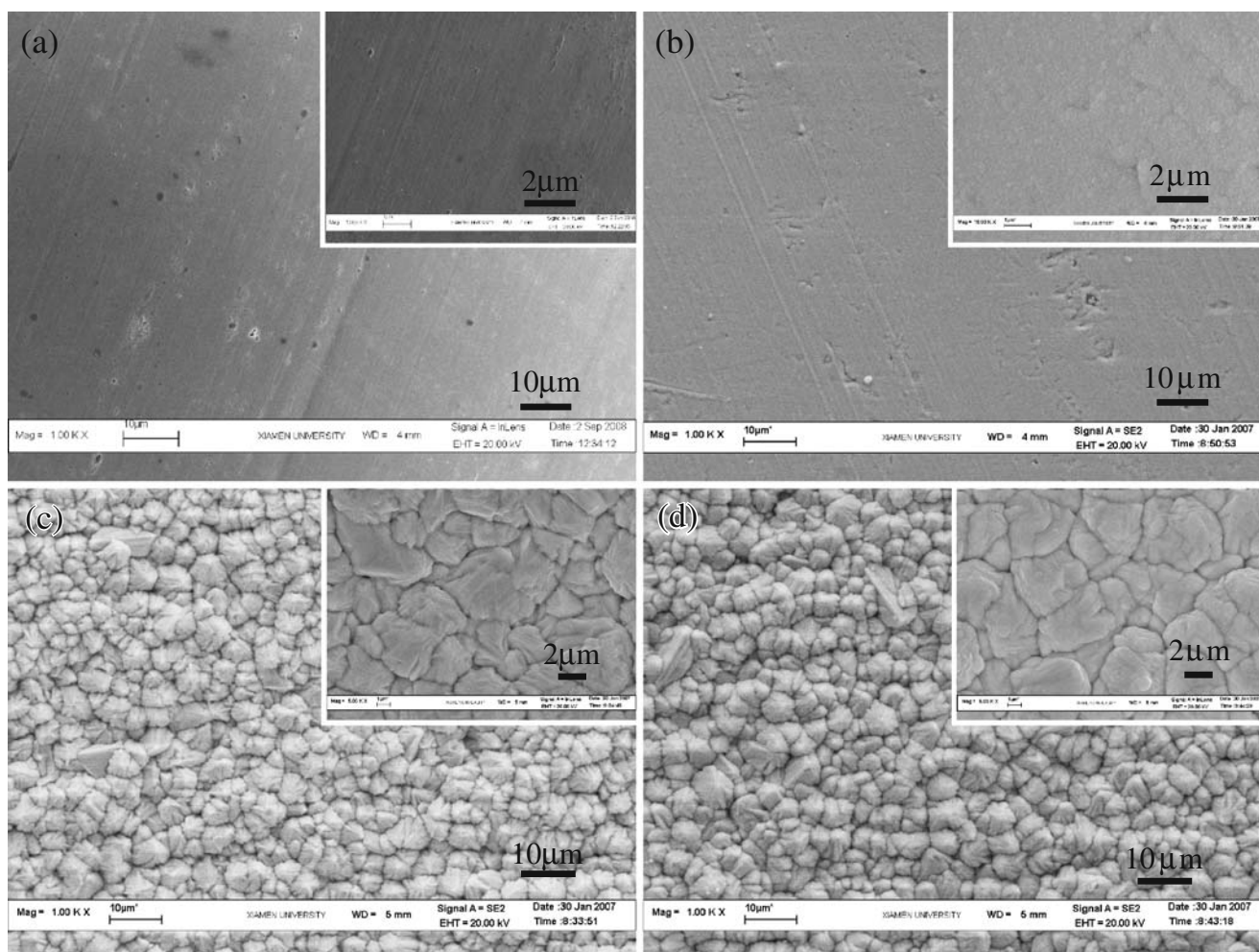
Fig. 1 SEM images of smooth Cu sheet (**a**), Sn–Co alloy (**b**) on the smooth Cu sheet, rough Cu foil (**c**), and Sn–Co alloy (**d**) on the rough Cu foil

rough Cu foil rapidly increases in initial three cycles and then gradually increases up to the 16th cycle, which can be attributed to the activation of active materials in initial 16 cycles. After 16 cycles, the charge capacity begins to gradually decrease until the 70th cycle. The capacity retention of the Sn–Co alloy electrode on the rough Cu foil after 70 cycles is determined to be as high as 80.0% (compared with the maximal capacity). The first coulomb efficiency (Fig. 3b) is measured at 73.7%, then rapidly increases to 92.9% starting from the second cycle and reaches its maximum (97.5%) in the seventh cycle. After seven cycles, the coulomb efficiency gradually decreases to 91.2% in the 44th cycle and gradually increases again from the 45th cycle until the 70th cycle.

For comparison, we have examined the charge/discharge performance of the Sn–Co alloy electrode on the smooth Cu sheet, and the results are illustrated in Fig. 4. It can be observed from Fig. 4a that the Sn–Co alloy electrode on the smooth Cu sheet has the similar charge/discharge curve shapes to that of the Sn–Co alloy electrode on the rough Cu

foil, and the first discharge and charge capacity is measured at 550.5 and 450 mAh g^{-1}, respectively. Since there is large volume expansion during lithiation, lithiated active materials stretch sidewards and trap some fresh active materials in the gaps between the "islands" on the surface of Sn–Co alloy electrode on the rough Cu foil. As a result, the lithium ions have to transfer in a longer channel, then the capacity of the Sn–Co alloy electrode on the rough Cu foil cannot be fully released in the first cycle, so the first charge/discharge capacity is a little smaller than that of the Sn–Co alloy electrode on the smooth Cu sheet. Although the first charge/discharge capacity of the Sn–Co alloy electrode on the smooth Cu sheet is larger than that of the Sn–Co alloy electrode on the rough Cu foil, its capacity fading rate is much larger than that of the Sn–Co alloy electrode on the rough Cu foil. After ten electrochemical cycles, the charge and discharge capacities are rapidly decreased to 99.5 and 107.5 mAh g^{-1}, respectively, in the 50th cycle.

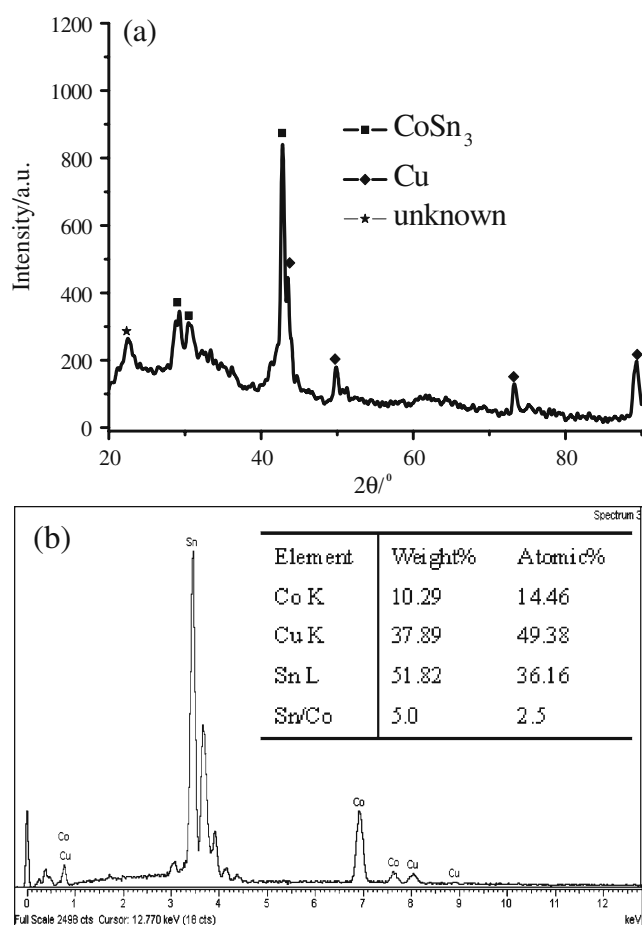Figure 5 displays the SEM images of the Sn–Co alloy electrode on the rough Cu foil after first full discharging (a),

Fig. 2 XRD patterns and EDS result of as-deposited Sn–Co alloy on the rough Cu foil

Fig. 3 Charge and discharge curves (**a**) and cycleability curves (**b**) of the Sn–Co alloy electrode on the rough Cu foil

one cycle (b), five cycles (c), ten cycles (d), 20 cycles (e), and 50 cycles (f). After first full discharging (Fig. 5a), the gaps between the small "islands" on the electrode surface are almost filled up due to the active materials stretch upwards and sidewards caused by the volume expansion during lithiation, and consequently, the surface of the Sn–Co alloy electrode on the rough Cu foil becomes smooth. When the Sn–Co alloy electrode on the rough Cu foil is charged/discharged one cycle (Fig. 5b), the surface is divided into many small "islands" again, which indicates that this surface morphology of the Sn–Co alloy electrode can reversibly expand and contract to some extent during charging/discharging. This reversibility of surface morphology changes of the Sn–Co alloy electrode on the rough Cu foil can protect the active materials from sticking out and peeling off the foil, which is one main reason of improving the cycleability. Meanwhile, we can also observe that the "islands" on the electrode surface suffering one cycle becomes more outstanding (see inset to Fig. 5b) compared with the as-deposited one (see inset to Fig. 1d). This result indicates that the active materials squeeze out and cannot fully contract to the same volume to the as-deposited one
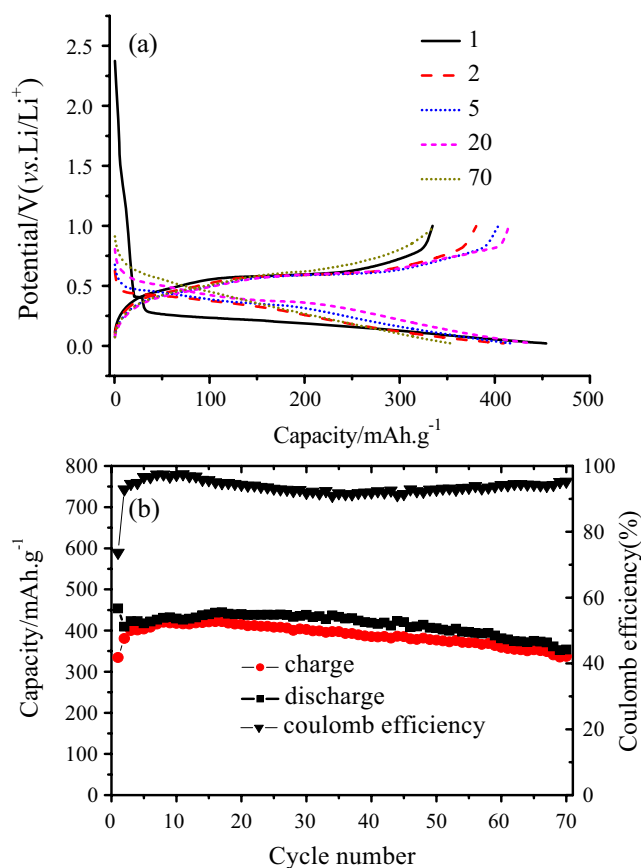
owing to the volume expansion. After five cycles (Fig. 5c), the outstanding "islands" on the surface of the Sn–Co alloy electrode become flat compared with that of the Sn–Co alloy electrode suffering one cycle, which maybe caused by reconfiguration of active materials during cycling due to high mobility of Sn atom in the Sn–Co alloy. After ten cycles (Fig. 5d), there begins to appear many cracks on each "island" of the Sn–Co alloy electrode surface and is gradually split into many smaller "islands". This phenomenon persisted until the 20th cycle (see Fig. 5e), which demonstrates that there appears further reconfiguration on the electrode surface. After 70 cycles (Fig. 5f), the electrode surface becomes smooth, and no obvious cracks can be detected because the surface cannot contract again after many times of expansion and contraction. Through above analysis, it can be concluded that although the surface of the Sn–Co alloy electrode suffered huge changes, the active materials can be well adhered to the substrate and provide good electronic contact with the substrate, which is one main reason for improving the cycleability discussed above.

For comparison, the SEM images of the Sn–Co alloy electrode on the smooth Cu sheet after first lithiation, one cycle, five cycles, and 20 cycles are shown in Fig. 6. After first lithiation (Fig. 6a), there appear many ruleless holes on
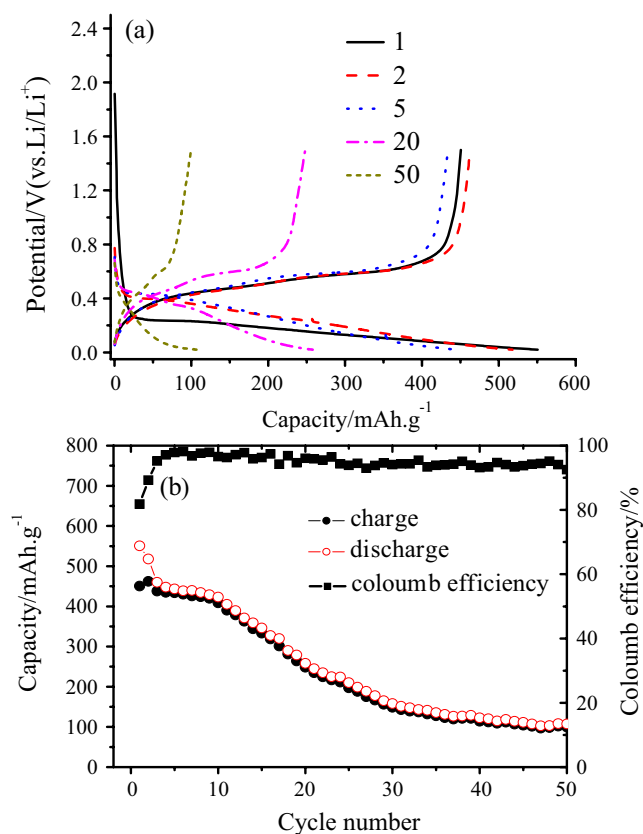
Fig. 4 Charge and discharge curves (**a**) and cycleability curves (**b**) of the Sn–Co alloy electrode on the smooth Cu sheet

the surface of the Sn–Co alloy electrode on the smooth Cu sheet owing to no "islands" and gaps existing on the surface accommodate the volume expansion. After one cycle (Fig. 6b), there appear many cracks on the surface of the Sn–Co alloy electrode on the smooth Cu sheet, and these cracks become more obvious after five cycles (Fig. 6c). After 20 cycles (Fig. 6d), it can be observed that there are some active materials peeled off from the electrode surface, which causes failure of the Sn–Co alloy electrode.

Impedance technique is usually used for electrochemical systems that can reach true equilibrium state. Then, by perturbing the system from true equilibrium by a small ac current (or potential) at a variety of frequencies, one can identify the various relaxation processes (such as charge transfer, diffusion, etc.) which are the RDS in each characteristic frequency domain [13]. Figure 7 shows the typical impedance spectra of the Sn–Co alloy electrode on the rough Cu foil at different polarized electrode potential. It can be observed that the Nyquist plots at open electrode potential is characterized by a large arc in all the frequency region between 10^5 and 10^{-2} Hz, which presents the blocking electrode character of non-lithiated electrode at equilibrium electrode potential. When the electrode potential is negatively polarized to 1.1 V, there appears a new arc in high-

frequency region. When the electrode potential is negatively polarized to the electrode potential range from 0.4 to 0.15 V, it is most interesting that all Nyquist plots are characterized by three regions, i.e., high frequency arc, middle frequency arc, and low frequency arc. This result can be evidenced by their bode plots (see Fig. 8). It can be observed that there are three peaks in the bode plots, i.e., one peak in the frequency range from 10^5 to 10^2 Hz, another peak in the frequency range from 10^2 to 1 Hz, and the third peak in the frequency range from 1 to 10^{-2} Hz. In general, electrochemical kinetics characteristic for battery materials is represented by several common steps, including ionic and electronic conduction through surface layer of active material, reach on the particle interface, diffusion inside particles, and phase-transfer reaction in case of several phases are present [14]. Indeed, two-phase coexistence during ion insertion into host electrodes has been confirmed not only by appropriately designed in situ XRD characterizations [15, 16] but also, in suitable cases, by direct observation of the moving boundary, which indicated the different colors of the lithiated graphite in various stages (see [17]). Usually, impedance spectra of intercalation electrodes in the presentation of Nyquist plots comprise two semicircles: high-frequency semicircle, which relates to Li ions' migration through the surface films that cover the active mass, and a medium-frequency semicircle which is usually attributed to charge transfer of Li ions across the interface between the surface films and the active mass (R_{ct}, in parallel to an interfacial double layer capacitance, C_{dl}) [18–22]. In some cases, a third low-frequency semicircle may appear in the Nyquist plots. There are several viewpoints about the appearance of the third semicircle in the low-frequency region. Levi and Aurbach [23] have attributed the appearance of the third semicircle in the low frequency to the non-oriented electrodes comprising several types of particles and relatively low value of σ and κ when they investigated graphite electrode, which are highly porous with a poor orientation of their particles. Hong et al. [24] found that the phase transformation will occur only when the applied energy (such as using the potentiostatic amplitude of 10 or 30 mV other than usually 5 mV) is higher than opposing elastic–plastic accommodation energy determined by the volume change (between $LiFe_{0.9}Mg_{0.1}PO_4$ and $Li_{0.1}Fe_{0.9}Mg_{0.1}PO_4$, there is a 6.5% volume change) in the phase transformation when they investigated $LiFe_{0.9}Mg_{0.1}PO_4$ electrode. However, Barsoukov et al. [14] found that the phase transformation impedance arc can also appear when using lower frequency limit such as 10^{-3} Hz at the potentiostatic amplitude of 5 mV. Zhuang et al. [25] suggested that the middle- and low-frequency arc should be attributed to electronic impedance and charge transfer impedance when there appeared three arcs in Nyquist plots for the semiconductor electrode materials such as $LiCoO_2$ electrode.
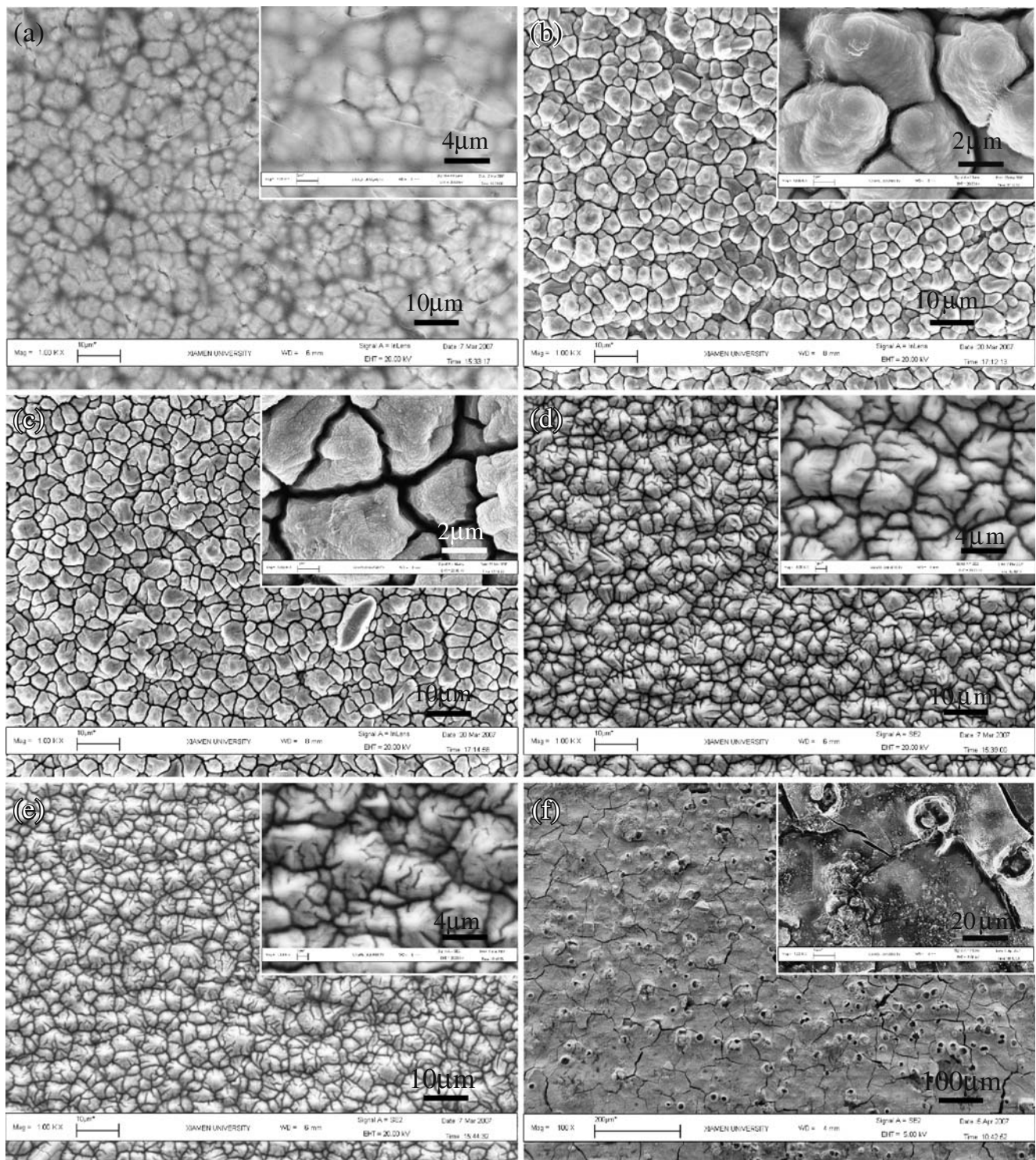
Fig. 5 SEM images of the Sn–Co alloy electrode on rough Cu Foil after first full discharge (**a**), one cycle (**b**), five cycles (**c**), ten cycles (**d**), after 20 cycles (**e**), and 70 cycles (**f**)

As for our experimental system in this paper, the particles of the Sn–Co alloy are uniform, so the appearance of low frequency arc cannot be attributed to the non-uniformity of particles. Meanwhile, the Sn–Co alloy electrode has high electronic conductivity, so the middle-

frequency arc representing electronic conductivity impedance could not be observed. Nevertheless, we note that phase transformation from Sn–Co alloy to Li_ySn ($y<4.4$) and serious volume expansion (usually larger than 100%) appear in first lithiation of the Sn–Co alloy electrode.
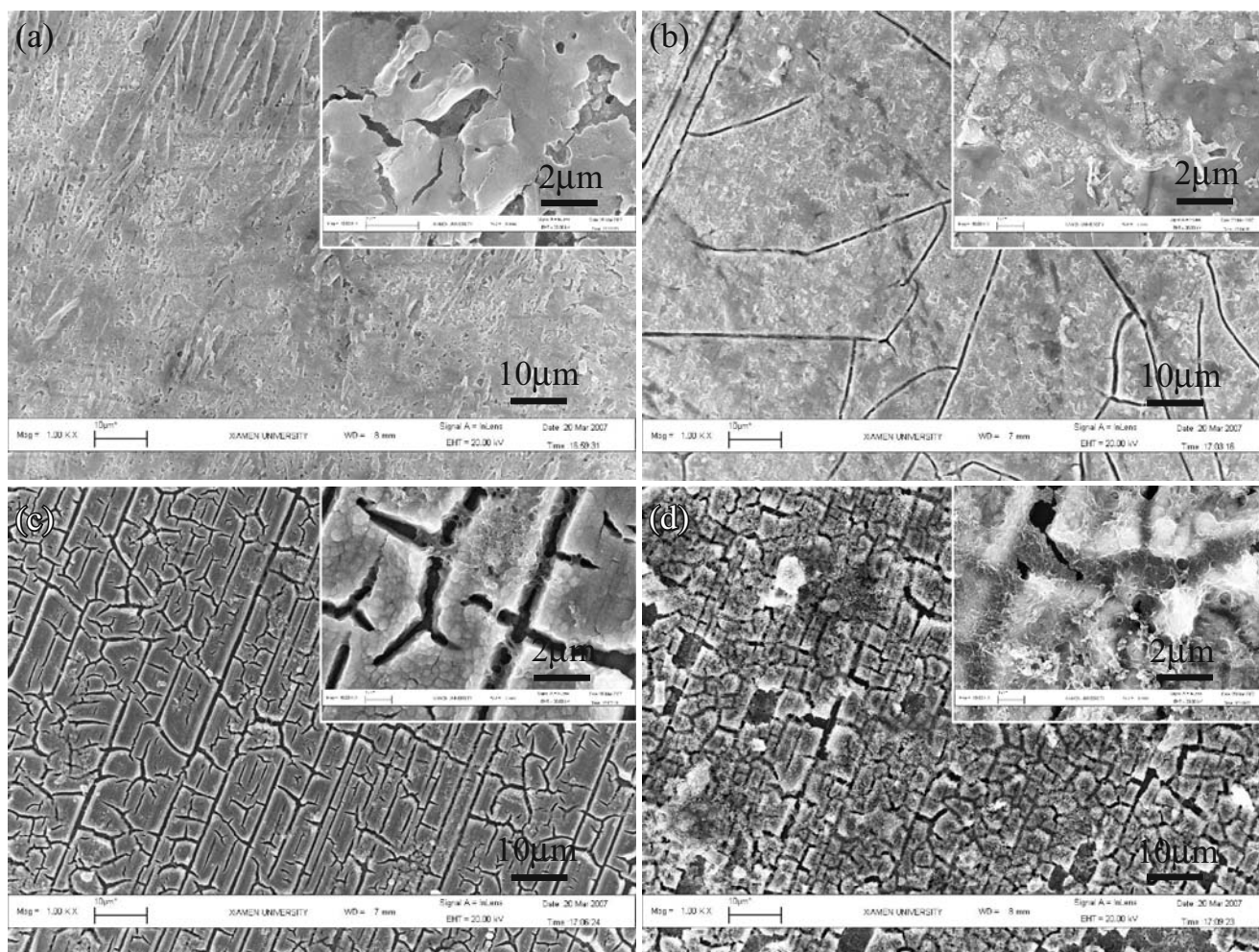
Fig. 6 SEM images of the Sn–Co alloy electrode on smooth Cu sheet after first full discharge (**a**), one cycle (**b**), five cycles (**c**), and 20 cycles (**d**)

Owing to the physical and chemical properties of the Sn–Co alloy phase and the lithiation phase (Li_ySn alloy) are much different, the transfer rates of lithium ion in the two phases demonstrate much difference. This much difference causes two separated time constants of lithium ion transfer in the Nyquist plots; a new arc which presented phase transformation impedance is detected in the low-frequency region [14]. This phenomena cannot be observed for common electrode materials (such as $LiCoO_2$, $LiMn_2O_4$, $LiFePO_4$, and graphite) because there are not enough volume expansion (usually <10%) during cycling; as a result, no obvious phase boundary appears between two phases during lithiation or delithiation. Meanwhile, it can be observed that the middle-frequency arc disappears when the electrode potential is decreased below 0.125 V due to the charge transfer impedance decreases too small to be detected in Nyquist plots.

To evaluate the variation of impedance spectra quantitatively, one equivalent circuit shown in Fig. 9 is proposed to fit the EIS data of the Sn–Co alloy electrode on the rough Cu foil. In this equivalent circuit, R_s represents the ohmic resistance, R_{SEI}, R_{ct}, and R_p are the resistances of the SEI film, the charge transfer, and phase transformation, respectively. The capacitance of the SEI film, the double layer, and the phase formation are presented by the constant phase elements (CPE) Q_{SEI}, Q_{dl}, and Q_p, respectively. The expression for the admittance response of the CPE (Q) is:

$$Y = Y_0\omega^n \cos\left(\frac{n\pi}{2}\right) + jY_0\omega^n \sin\left(\frac{n\pi}{2}\right), \quad (1)$$

where ω is the angular frequency and j is the imaginary unit. A CPE represents a resistor when $n=0$, a capacitor with capacitance of C when $n=1$, an inductor when $n=-1$, and a Warburg resistance when $n=0.5$. In this study, Y_0 is considered to be a pseudo-capacitance (pseudo-Y_0) [26].

A typical simulation result and experimental data at the electrode potential of 0.375 V are shown in Fig. 10. Comparing the two curves, we can conclude that they are fitted well.
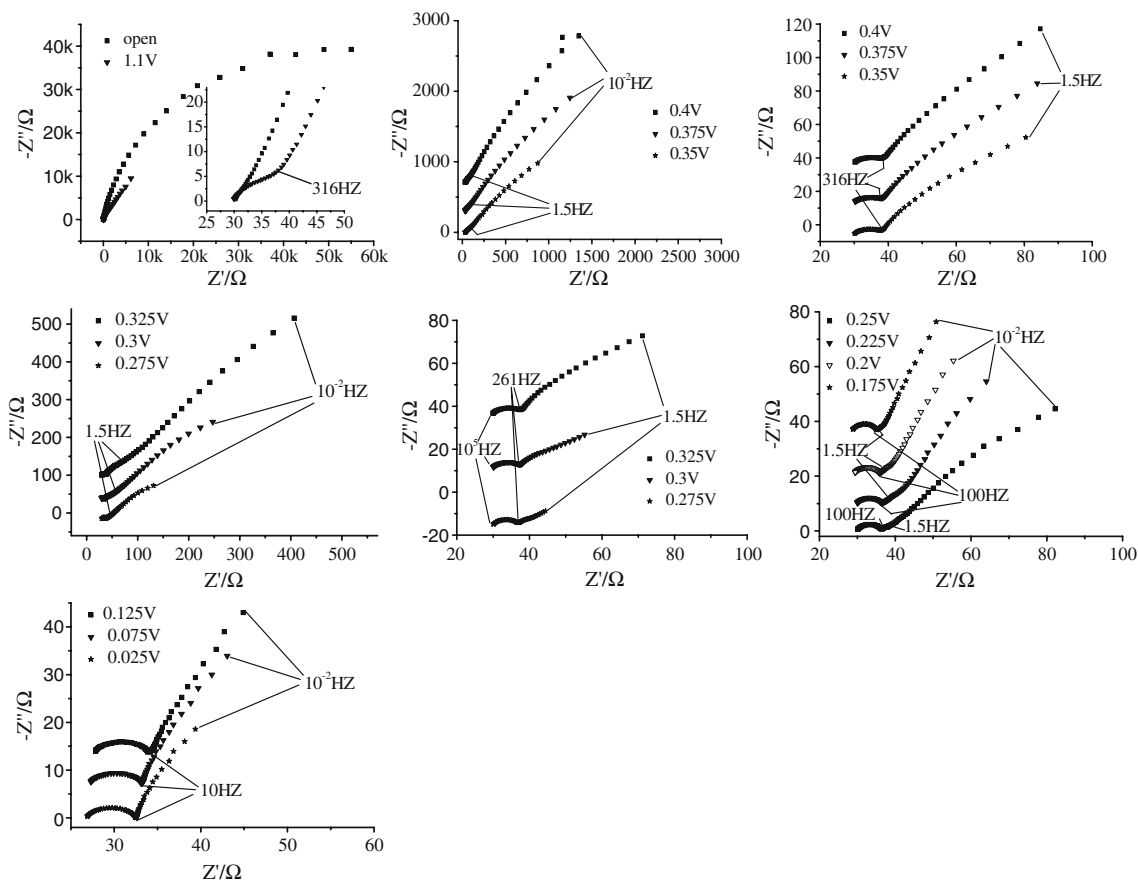
Fig. 7 Nyquist plots of the Sn–Co alloy electrode on the rough Cu foil in first lithiation

Figure 11 illustrates the variations of R_{SEI}, R_{ct}, and R_p vs. the electrode potentials obtained by fitting the experimental impedance spectra of the Sn–Co alloy electrode on the rough Cu foil. It can be observed that the R_{SEI} increase upon decreasing of the electrode potential in the range from 0.8 to

0.6 V, which indicates that the SEI film gradually grows thicker in the electrode potential range owing to the electrolyte decomposition on the electrode surface. It can be also observed that the R_{SEI} rapidly decreases upon negatively polarizing to the electrode potential range from 0.6 to 0.275 V. As we know, there are large amount of lithium ions inserted into the Sn–Co alloy in the electrode potential range from 0.6 to 0.275 V; consequently, large volume expansion appears. The large volume expansion causes the SEI film partially breaking, and fresh electrode surface is exposed, then the R_{SEI} decreases [27]. In the electrode potential range from 0.275 to 0.2 V, the electrolyte is decomposed again on the fresh electrode surface produced by SEI breakage, so the R_{SEI} increases again upon decreasing of the electrode potential. When the SEI film on the electrode surface suffered breaking and repairing, it becomes almost stable and decreases slightly upon decreasing of electrode
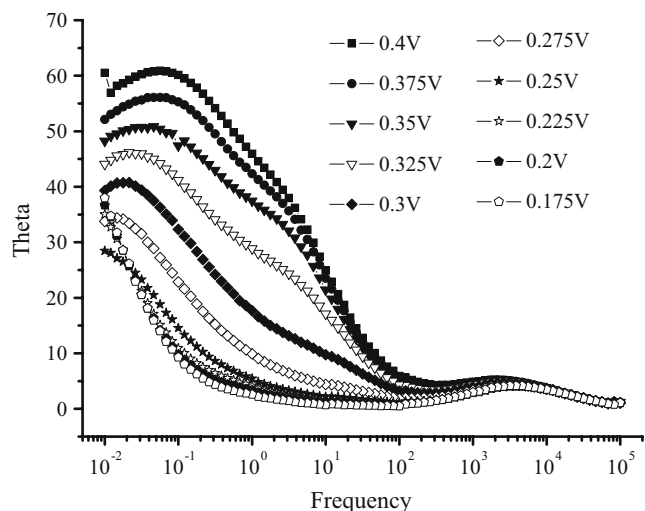

Fig. 8 Bode plots of the Sn–Co alloy electrode on the rough Cu foil at the electrode potential range between 0.4 and 0.175 V
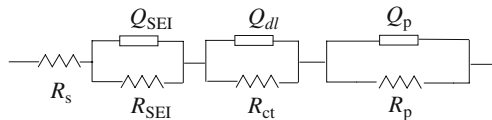

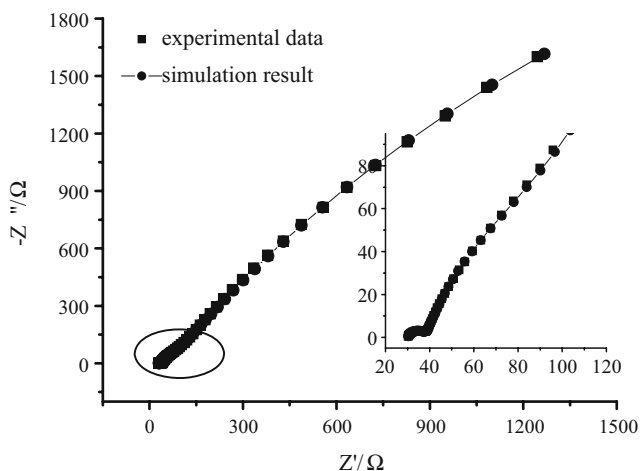**Fig. 9** Equivalent circuit of EIS of the Sn–Co alloy electrode on rough Cu foil

Fig. 10 EIS data and simulation result of the Sn–Co alloy electrode on rough Cu foil at the potential of 0.375 V

rapidly upon decreasing of the electrode potential, which reveals that an obvious phase transformation process appears in the electrode potential range. When the electrode potential is decreased below 0.25 V, R_p increases upon decreasing of the electrode potential, which indicates that phase transformation begins to disappear at this electrode potential range. When the electrode potential is polarized below 0.175 V, due to the appearance of a new phase transformation process, the R_p decreases again upon decreasing of the electrode potential. This result is consistent with the result obtained by Barsoukov et al. who found that the resistance, R_p, which is related to phase growth, decreases with beginning of a new phase formation initially and remains almost constant until, at complete discharged state, it again reaches very high values.

Conclusion

Sn–Co alloy electrode was prepared on different substrates by electrodepositing. The cycleability of the Sn–Co alloy electrode on the rough Cu foil as for anode of lithium-ion battery was proved to be significantly better compared with that of the Sn–Co alloy electrode on the smooth Cu sheet. The charge capacity can retain 80.0% of the maximal capacity after 70 cycles. The excellent capacity retention of the Sn–Co alloy on the rough Cu foil can be contributed to buffering

potential owing to volume expansion when the electrode potential is decreased below 0.2 V. From Fig. 11b, we can observe that R_{ct} decreases when the electrode potential is negatively polarized into the range of main discharging region (from 0.325 to 0.0 V), which indicates the typical character of charge transfer impedance.
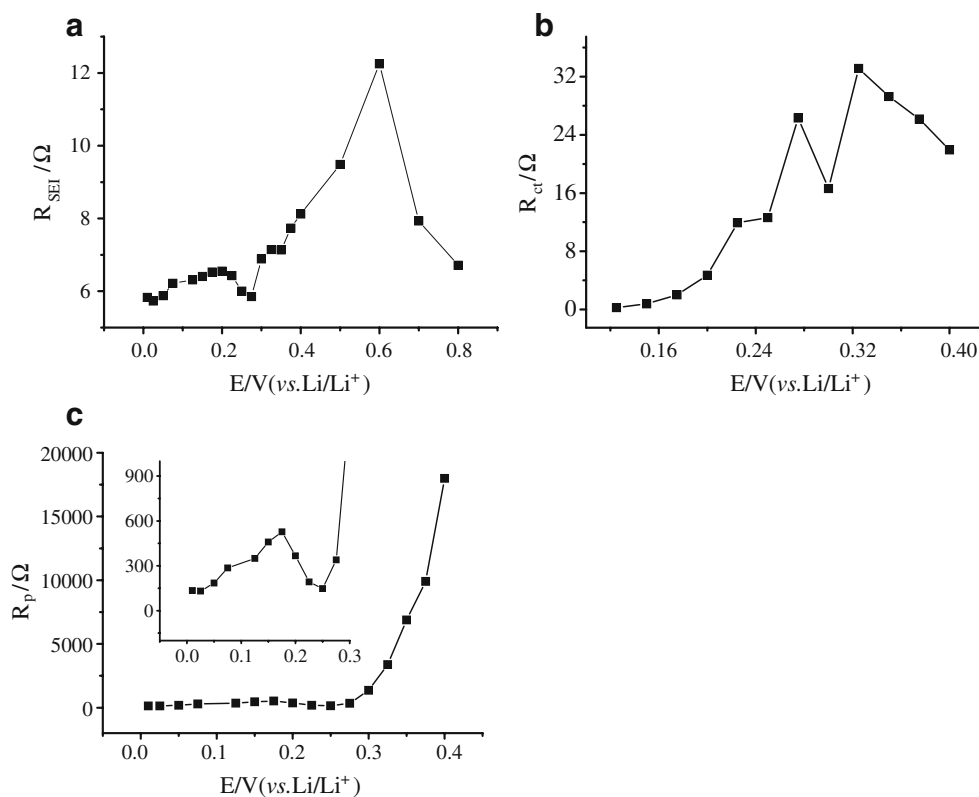
Figure 11c displays the evolution of phase transformation resistance, R_p, versus the electrode potential. When the electrode potential is larger than 0.25 V, the R_p decreases

Fig. 11 R_{SEI}, R_{ct}, and R_p of the Sn–Co alloy electrode on rough Cu foil versus electrode potential

volume expansion and good electronic contact with active materials of its unique surface structure illustrated in the SEM images at different charging/discharging status. Through EIS examination, the SEI film and charge transfer and their changing principle were studied. In addition, phase transformation process was also detected in the electrochemical impedance spectra, and its evolution principle was proved to be similar to that of the charge/discharge process.

References

1. Idota Y, Kubota T, Matsufuji A, Maekawa Y, Miyasaka T (1997) Science 276:1395. doi:10.1126/science.276.5317.1395
2. Besenhard JO, Yang J, Winter M (1997) J Power Sources 68:87. doi:10.1016/S0378-7753(96)02547-5
3. Winter M, Besenhard JO (1999) Electrochim Acta 45:31. doi:10.1016/S0013-4686(99)00191-7
4. Kepler KD, Vaughey JT, Thackray MM (1999) J Power Sources 81–82:383. doi:10.1016/S0378-7753(99)00111-1
5. Catia A, Mariachiara L, Marina M (2005) J Electrochem Soc 152:A289. doi:10.1149/1.1839466
6. Wanuk C, Jeong LY, Hong SL (2004) Electrochem Commun 6:816. doi:10.1016/j.elecom.2004.05.018
7. Thackeray MM, Vaughey J, Kahaian AJ, Kepler KD, Benedek R (1999) Electrochem Commun 1:111. doi:10.1016/S1388-2481(99)00018-1
8. Beattie SD, Dahn JR (2003) J Electrochem Soc 150:A894. doi:10.1149/1.1577336
9. Tamura N, Fujimoto M, Kamino M, Fujitani S (2004) Electrochim Acta 49:1949. doi:10.1016/j.electacta.2003.12.024
10. Tamura N, Kato Y, Mikami A, Kamino M, Matsuta S, Fujitani S (2006) J Electrochem Soc 153:A1626. doi:10.1149/1.2205156
11. Zhang JJ, Xia YY (2006) J Electrochem Soc 153:A1466. doi:10.1149/1.2204871
12. Ionica-Bousquet CM, Lippens PE, Aldon L, Olivier-Fourcade J, Jumas JC (2006) Chem Mater 18:6442. doi:10.1021/cm062132i
13. Levi MD, Aurbach D (2007) J Solid State Electrochem 11:1031. doi:10.1007/s10008-007-0264-x
14. Barsoukov E, Kim JH, Kim DH, Hwang KS, Yoon CO, Lee H (2000) J Mater Electrochem Syst 3:301
15. Dahn JR (1991) Phys Rev B 44:9170. doi:10.1103/PhysRevB.44.9170
16. Ohzuku T, Iwakoshi Y, Sawai K (1993) J Electrochem Soc 140:2490. doi:10.1149/1.2220849
17. Funabiki A, Inaba M, Abe T, Ogumi Z (1999) J Electrochem Soc 146:2443. doi:10.1149/1.1391953
18. Chusid O, Ein-Eli Y, Aurbach D et al (1993) J Power Sources 43:47. doi:10.1016/0378-7753(93)80101-T
19. Levi MD, Aurbach D (1997) J Phys Chem B 101:4630. doi:10.1021/jp9701909
20. Aurbach D, Levi MD, Levi E, Schechter A (1997) J Phys Chem B 101:2195. doi:10.1021/jp962815t
21. Markovsky B, Levi MD, Aurbach D (1998) Electrochim Acta 43:2287. doi:10.1016/S0013-4686(97)10172-4
22. Barsoukov E, Kim JH, Kim DH, Yoon CO, Lee H (1999) Solid State Ion 116:249. doi:10.1016/S0167-2738(98)00411-1
23. Levi MD, Aurbach D (2005) J Power Sources 146:727. doi:10.1016/j.jpowsour.2005.03.164
24. Hong J, Wang CS, Kasavajjula U (2006) J Power Sources 162:1289. doi:10.1016/j.jpowsour.2006.08.004
25. Zhuang QC, Xu JM, Fan XY, Dong QF, Jiang YX, Huang L, Sun SG (2007) Chin Sci Bull 52:147. doi:10.1007/s11434-007-0169-1
26. Kim YO, Park SM (2001) J Electrochem Soc 148:A194. doi:10.1149/1.1345870
27. Fan XY, Zhuang QC, Jiang HH, Huang L, Dong QF, Sun SG (2007) Acta Chimi Sin 65:165